Optics Communications 356 (2015) 362–367

Contents lists available at ScienceDirect

Optics Communications

journal homepage: www.elsevier.com/locate/optcom

Multi-band near-perfect absorption via the resonance excitation of dark meta-molecules

Bui Son Tung [a], Bui Xuan Khuyen [a], Nguyen Van Dung [a], Vu Dinh Lam [b], Yong Hwan Kim [c], Hyeonsik Cheong [d], YoungPak Lee [a,*]

[a] Department of Physics, Quantum Photonic Science Research Center and RINS, Hanyang University, Seoul 133-791, South Korea
[b] Institute of Materials Science, Vietnam Academy of Science and Technology, Hanoi, Vietnam
[c] Infovion Inc., Seoul, South Korea
[d] Sogang University, Seoul, South Korea

ARTICLE INFO

Article history:
Received 14 June 2015
Received in revised form
4 August 2015
Accepted 10 August 2015

Keywords:
Metamaterial
Perfect absorption
Electromagnetic-induced transparency

ABSTRACT

We numerically study a multi-band absorption based on electromagnetic-induced-transparency effect of metamaterial. By exploiting the coupling between bright and dark plasmonic modes of cut-wire triplet, which consists of a vertical wire and two horizontal wires, a dual-band absorption is realized at 243 and 266 THz. Then, the absorber structure is improved by adding two new horizontal wires which play role as second dark meta-molecules. Due to the dark–dark coupling, another absorption band arises so that a triple-band absorption is created at 240, 250 and 264 THz. The role of interaction between dark meta-molecules in triple-band absorption is investigated, revealing a specific non-monotonic characteristic of the second absorption peak. Finally, the influence of incident angle of EM wave on multi-band absorbers shows that the absorption of lowest frequency peak is robust while those of higher frequency peaks are strongly weaken with increasing of the incident angle.

1. Introduction

Artificial sub-wavelength materials, the so-called metamaterials (MMs), can exhibit desirable electromagnetic (EM) responses which are even not found in natural materials. By tailoring the unit-cell structure, a variety of fascinating phenomena are realized such as negative refractive index [1–3], invisibility cloaking [4,5], and super-resolution [6,7]. In 2008, another attractive phenomenon, which is perfect absorption, was discovered by Landy et al. [8] and made a lot of attention due to the considerable amount of applicability in devices including solar cells [9], imaging [10], and plasmonic sensor [11]. Since then, researches on MM perfect absorber (MPA) have been expanded, bringing many demonstrations in various frequency ranges [12–14]. Nowadays, multi-band and broadband absorption are still the focus of interest for real needs. A common approach is to design a geometrically gradient multi-resonator structure whose resonances, separated closely, can be directly and simultaneously excited by the incident wave [15–17].

Electromagnetic-induced transparency (EIT) is basically a quantum coherent process which requires very complicated and rigorous experimental conditions [18,19]. One of the superiorities of MMs is that the EIT effect can be mimicked in a much more easier way by using MMs [20–22]. In this work, a different approach to create a multi-band MPA is proposed by exploiting the EIT effect. Generally, there is single absorption peak when external EM field excites only one plasmonic resonance. The key idea is that dual-band absorption can be achieved by employing the near-field coupling between bright and dark plasmonic modes even though only one resonance can be directly excited by the EM field. An extended model inducing triple-band absorption is also provided by considering the interaction between dark meta-molecules. Finally, the role of dark–dark coupling in absorption spectrum is studied to comprehend the EM behavior of multi-band MPA. Our work might be useful for many applications such as multi-frequency filters and single/multi-mode switching devices.

2. Design and simulation

Fig. 1 illustrates the unit cell structures of designed cut-wire-triplet (CWT) and cut-wire-quintet (CWQ) absorbers. The CWT absorber (CWTA) structure is made of three different layers. The front layer is a metallic CWT which consists of a vertical cut wire (CW) and two horizontal CWs placed at a certain distance from the ends of the vertical. The geometry of these CWs is identical. The middle and back layers are continuous dielectric and metallic

* Corresponding author.
E-mail address: yplee@hanyang.ac.kr (Y. Lee).

http://dx.doi.org/10.1016/j.optcom.2015.08.022
0030-4018/

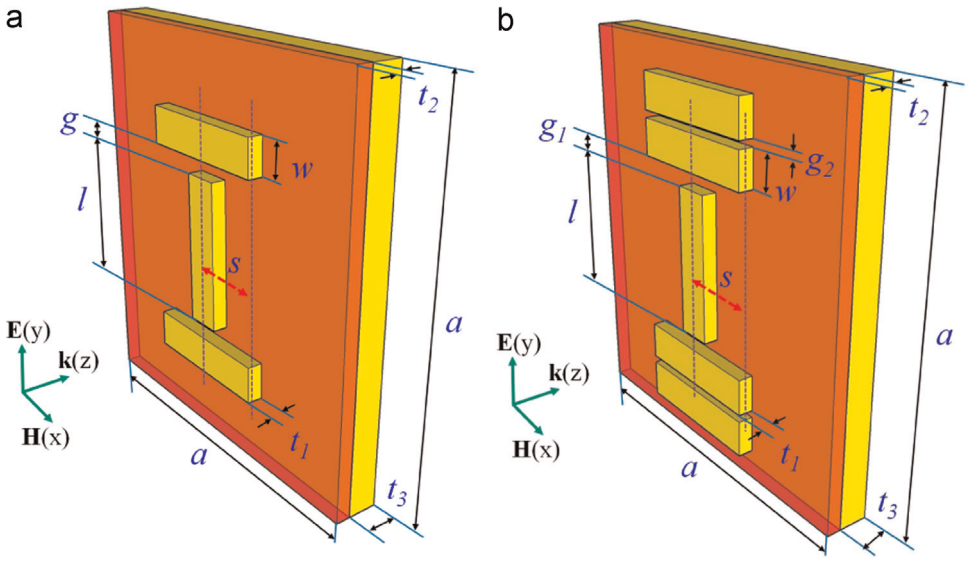

Fig. 1. Illustrations of the unit cell of (a) cut-wire-triplet and (b) cut-wire-quintet absorbers with the electromagnetic polarization.

plane, respectively. The detailed geometrical parameters of CWTA are $a=800$ nm, $t_1=t_2=30$ nm, $t_3=100$ nm, $l=190$ nm, $w=80$ nm, and $g=20$ nm. The CWQ absorber (CWQA) structure is an extended structure of CWTA by adding one more pair of horizontal CWs on the front layer. The CWQA has the same geometrical parameters as CWTA except two new parameters $g_1=20$ nm and $g_2=10$ nm. The parameter s defines the displacement of the vertical CW from the center position. This parameter is a key factor to achieve a multi-band absorption.

In our simulation, the metal was silver and described by the Drude model, with a plasmon frequency of 1.366×10^{16} rad s^{-1} and a collision frequency of 3.07×10^{13} Hz [20,23]. The dielectric was chosen as silicon dioxide with the function fitted from Ref. [24]. The simulations were performed using a finite-integration

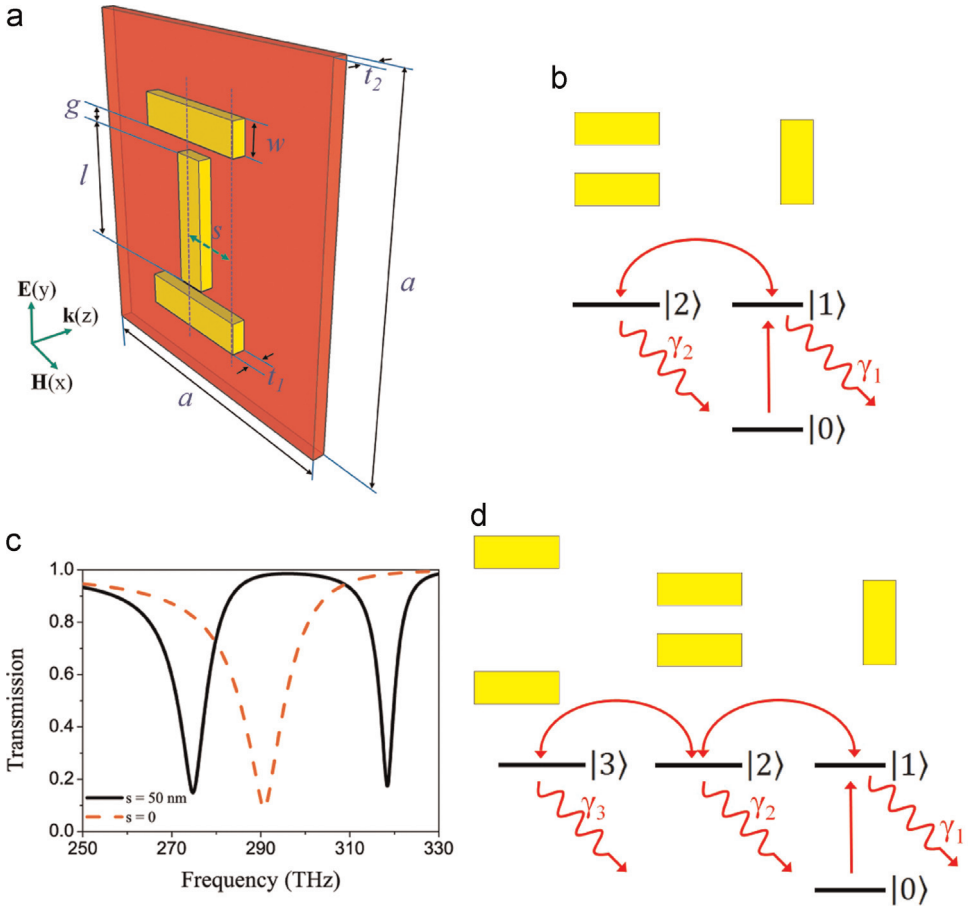

Fig. 2. (a) Illustration of the unit cell of EIT structure with the electromagnetic polarization. (b) Schematic energy-level diagram of the cut-wire triplet. (c) Transmission spectra of the EIT structure according to s. (d) Schematic energy-level diagram of the cut-wire quintet.

package (CST Microwave Studio [25]). The boundary condition was applied so that the structures were periodic along the x and y directions. The EM wave propagation was normal to the structures with the electric and the magnetic fields that were polarized along the vertical and the horizontal CWs, respectively. The absorption was calculated as $A(\omega) = 1 - |S_{11}(\omega)|^2 - |S_{21}(\omega)|^2$, where $S_{11}(\omega)$ and $S_{21}(\omega)$ are the reflection and transmission parameters, respectively. For the real fabrication, the sample can be prepared using the lithography technique [26,27].

3. Results and discussion

3.1. Multi-resonance based on the electromagnetic-induced transparency

In this section, we explained how a multi-resonance can be excited by exploiting the EIT phenomenon. Fig. 2(a) presents an EIT structure which consists of only the CWT layer and the dielectric layer. It is well known that the vertical CW serves as a bright mode which is strongly coupled to the incident EM field while the two horizontal ones are weakly coupled and considered as the dark mode. Nevertheless, the dark mode can be excited by the bright mode through displacement s of the vertical CW. As shown in Fig. 2(b), two different excitation pathways, direct one $|0\rangle \rightarrow |1\rangle \rightarrow |0\rangle$ and indirect one $|0\rangle \rightarrow |1\rangle \rightarrow |2\rangle \rightarrow |0\rangle$, are destructively interfered that create a transparency window. This phenomenon is well known as the EIT effect. Fig. 2(c) shows the transmission spectra of EIT structure according to s of the vertical CW. In the case of $s=0$, a transmission dip locates at 290 THz which corresponds to excitation of the bright mode. When $s=50$ nm, a transmission band emerges at the position of the former dip and lies between two new transmission dips at 274 and 319 THz. However, for the purpose of creating a multi-band MPA by exploiting the EIT phenomenon, we paid attention to the two resonances instead of the transparency window. It is noteworthy that the number of these near-field-excited resonances depends on the number of dark modes of the EIT structure. Fig. 2 (d) presents an extended energy-level diagram using CWQ structure. As shown in Fig. 2(d), the dark–dark coupling between horizontal wires should also be counted, besides the normal bright–dark coupling between vertical and horizontal wires in the total EIT effect. Consequently, the CWQ structure will behave like a four-level meta-atom configuration, and the second transparency band can arise [28–30]. Therefore, it is possible to obtain three plasmonic resonances by exploiting the EIT effect of CWQ structure. In addition, there are two advantages of this approach via EIT effect in comparison with the conventional approach using geometrically gradient multi-resonator structure. Firstly, the geometry of all resonators is identical that make the fabrication of the structure may be easier than geometrically gradient multi-resonator structure. Secondly, only the bright resonator can be excited by incident EM field. The dark resonators are excited via near-field coupling when breaking the structural symmetry. For this reason, our approach is possible to be applied to single-band/multi-band (or broadband) switching devices using mechanical MM systems,

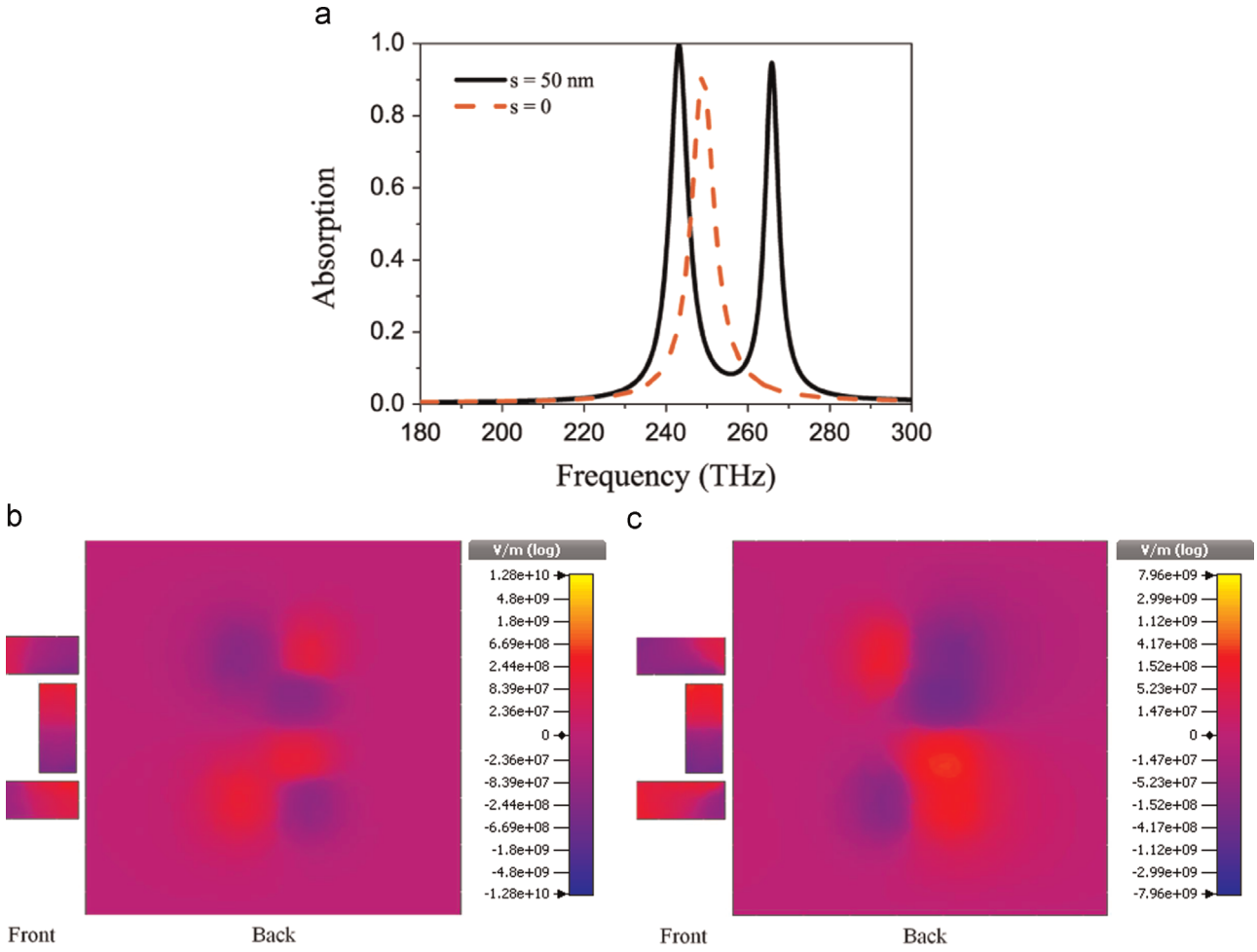

Fig. 3. (a) Absorption spectra of the cut-wire-triplet absorber according to s. Electric-field distributions at the front and the back silver layers of the cut-wire-triplet absorber at (b) 243 and (c) 266 THz.

where the dark resonators are fixed and the bright resonator is moveable.

3.2. Multi-band near-perfect absorption via the resonance excitation of dark meta-molecules

Based on the above discussion, we presented multi-band near-perfect absorbers using CWTA and CWQA structures. The absorption spectra of the CWTA according to s are demonstrated in Fig. 3(a). Initially, when the vertical wire is at the center, $s=0$, there is only one absorption peak at 249 THz with absorption of 90%. By breaking the structural symmetry, at $s=50$ nm, the initial absorption peak turns into a dual-band absorption with unity absorption at 243 THz and nearly perfect absorption of 94% at 266 THz. The observed dual-band absorption is the result of coupling between the CWT, which provides two resonances based on EIT effect, and the continuous plane. The absorption mechanism is further clarified by investigating the electric-field distributions at the front and the back layers of CWTA, as shown in Figs. 3(b) and 3(c), respectively. The coupling between the CWT and the back plane leads to a strong magnetic response which is indicated by the opposite charge distribution between the front wires and the back plane. Consequently, the EM field is trapped at 243 and 266 THz. It is noteworthy that the absorption resonances in CWTA, which are the magnetic resonances aforementioned, are different from the fundamental plasmonic resonances in Fig. 2(c). This is the reason why the dual-band absorption occurs at lower frequencies than the frequencies of original resonances caused by the EIT structure. The coupling between CWT layer and back plane in CWTA is similar to the magnetic response of the well-known CW-pair MM [31].

In order to prove the efficiency of our proposed approach in producing multi-band absorption, a more sophisticated model was investigated by extending the coupling scheme of EIT. Fig. 4(a) is the comparison of the absorption spectrum of CWQA with that of CWTA. The second absorption peak of CWTA at 266 THz is nearly unchanged with the same absorption of 94% except only slight shift to 264 THz in case of CWQA. However, the first absorption peak of CWTA at 243 THz is totally altered for the CWQA. This peak splits into two new absorption peaks at 240 and 250 THz

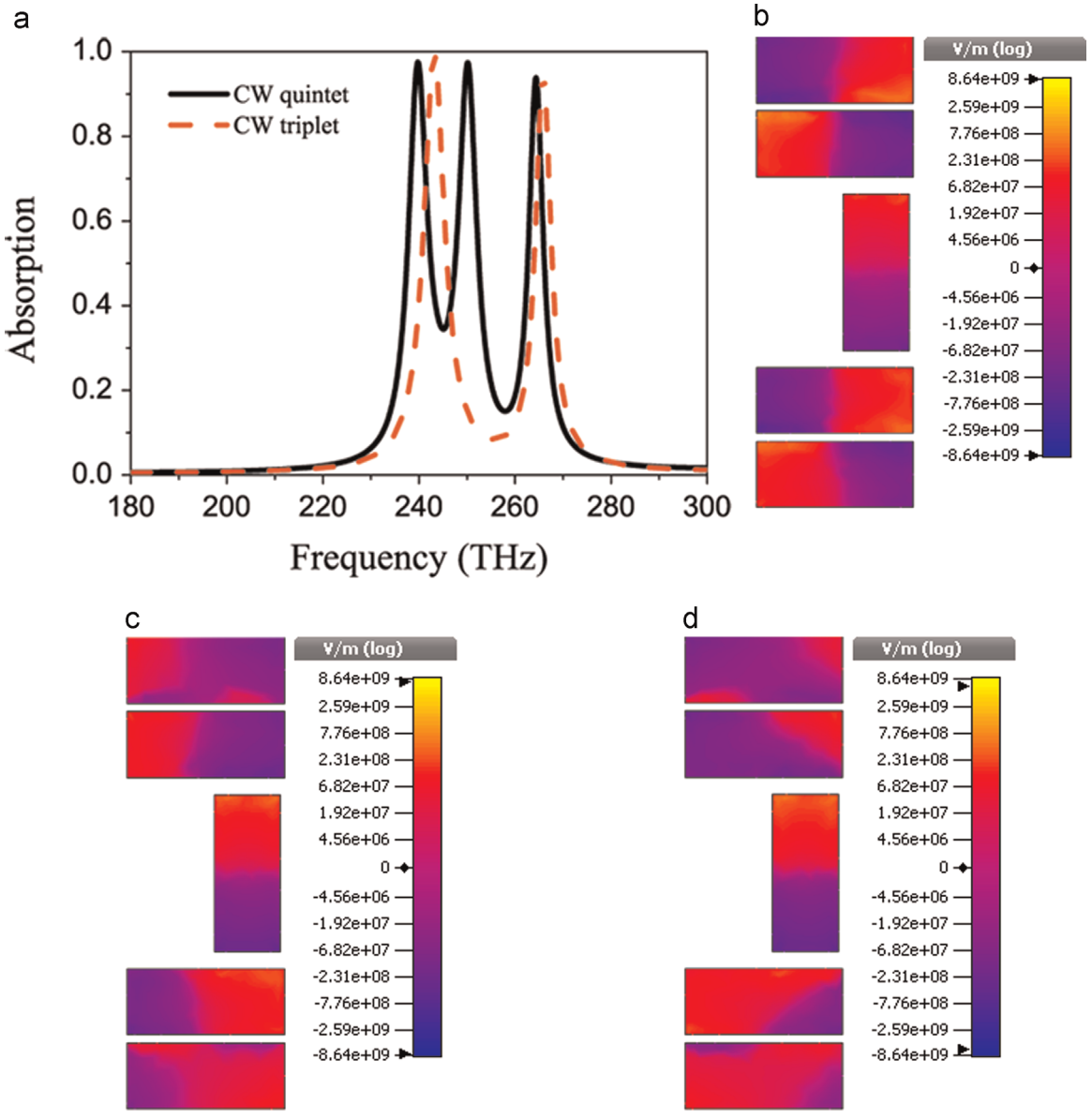

Fig. 4. (a) Absorption spectra of the cut-wire-quintet and -triplet absorbers when $s=50$ nm. Electric-field distributions at the front layer of the cut-wire-quintet absorber at (b) 240, (c) 250 and (d) 264 THz.

with absorption of 97%. In order to elucidate the mechanism of triple-band absorption, the electric-field distributions on the CWQ at the absorption frequencies are demonstrated in Figs. 4(b), 4(c) and 4(d). Obviously, the electric-field distribution on the CWQ at 264 THz [in Fig. 4(d)] and that on the CWT at 266 THz [in Fig. 3(c)] are similar. The charges on two additional horizontal CWs simply oscillate in phase with the adjacent original ones. Due to the unchanged coupling, this absorption peak of CWQA is nearly identical to the corresponding one of CWTA in both amplitude and frequency. The split of the absorption peak of CWTA at 243 THz into two absorption peaks of CWQA at 240 and 250 THz is also clarified in Figs. 4(b) and 4(c). In CWQ, the former CWT component [in Figs. 4(b) and 4(c)] still exhibits the same behavior of electric-field distribution as the CWT in Fig. 3(b), suggesting that the origin of the two absorption peaks of CWQA is the absorption peak of CWTA at 243 THz. However, the two additional horizontal CWs reveal totally different behavior due to the dark–dark coupling. Together with adjacent original horizontal CWs, the charge oscillations on CWs are in phase at higher frequency (250 THz) and out of phase at lower frequency (240 THz). The phenomenon is similar to the hybridization scheme of the well-known CW-pair MM and can also be considered as the hybridization effect [32]. The difference here is that the hybridization between in-plane adjacent horizontal CWs is only excited through the symmetry breaking of the structure. In case of the CWQA, the origin of nearly perfect absorption is still the magnetic resonance which is indicated by the opposite distribution of charges between the CWQ and the back metallic plane (which is not shown here). It is worthy to note that two dark modes were normally excited by using asymmetric elongated horizontal wires in previous research on the four-level EIT configuration [29,30]. In our work, we present that two dark resonances can be excited even by employing identical dark meta-molecules. However, the nature is still the same as before. To achieve the four-level configuration, one needs to create two separate dark modes. In our proposed structure, the two dark modes are separated by the different distances between bright and dark meta-molecules instead of using asymmetric dark meta-molecules.

The interaction between dark meta-molecules is studied for deeper understanding of the EM behavior of the multi-band absorption in CWQA. Fig. 5 presents the influence of distance g_2 between horizontal cut wires on absorption spectrum. When g_2 is changed from 10 to 50 nm, the absorption frequency of the first peak is blue-shifted from 240 to 244 THz while the near perfect absorption is maintained. The third absorption peak also exhibits a similar trend with the absorption frequency moved from 264 to 274 THz. However, the absorption is decreased with increasing g_2, which proves the weaker interaction between dark meta-molecules with separating the distance between them. On the other hand, the EM behavior of the second absorption peak is totally different. Initially, the peak is rapidly shifted from 250 to 258 THz and the absorption is strongly decreased when g_2 is varied from 10 to 15 nm. Further increase of g_2 leads to vanishing of the second peak. Then, it reappears at 261 THz for $g_2=18$ nm. When g_2 keeps increasing to 50 nm, the absorption is enhanced to be nearly 90% while the absorption frequency is unchanged. Our results are in accordance with the non-monotonic behavior of central resonance in four-level meta-atom configuration reported in Ref. [28]. However, here we observe a minimum of absorption instead of a maximum in that work. A possible explanation is due to the difference in structural design that is the presence of back metallic plane in our structure. Because of the coupling between back plane and front four-level meta-atom configuration of CWQ, the absorption behavior is reversed, leading to a minimum absorption for the second resonance.

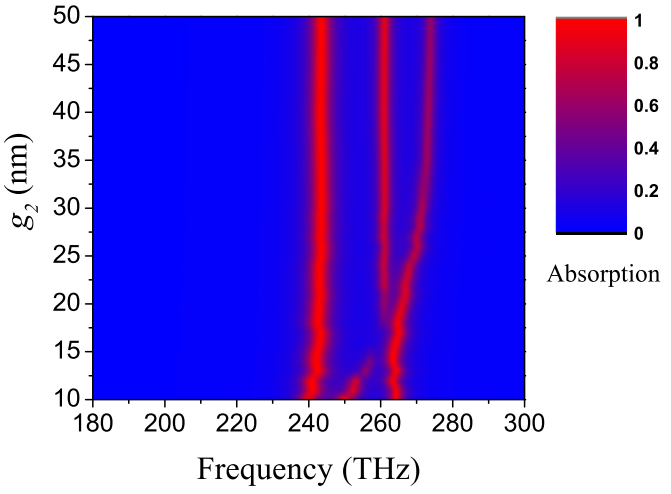

Fig. 5. Dependence of absorption spectrum on the distance g_2 between horizontal cut wires.

Since the dipole resonance (bright mode) in the vertical CW can be only strongly excited when the electric field is polarized along the length of CW, the proposed multi-band absorbers are much influenced by the EM polarization. Therefore, we have studied only the dependence of absorption spectra (for $s=50$ nm) on the incident angle θ of EM wave. In Fig. 6(a), the dual-band absorption of CWTA exhibits a slight red shift when θ varies from 0 to 40°. The first peak shows the nearly perfect absorption. However, for the second peak, the absorption is decreased by increasing the incident angle. The absorption comes to be only 78% when $\theta=40°$. A similar evolution is observed for the CWQA in Fig. 6(b). The triple-band absorption also exhibits a slight red shift and the rates of reduction in absorption are different for different absorption peaks. The absorption of first peak is slightly decreased and kept over 96% with increasing the incident angle up to 40°. The second peak is strongly influenced for the absorption to be decreased from 97% to 88%. For the third peak, the rate of reduction in absorption is the largest. The absorption of third peak is dramatically worsened from 94% to 74%.

4. Conclusions

We proposed a simple method to create multi-band MPA by exploiting the EIT effect. It is demonstrated that the dual-band absorption of CWTA due to the bright–dark coupling between the vertical CW and horizontal CWs. By using the CWQA, the EIT scheme is developed with the additional dark–dark coupling between adjacent horizontal CWs, which is used to obtain the triple-band absorption. Remarkably, the proposed approach can be extended by considering more coupling that will produce more absorption bands. In addition, a non-monotonic behavior of the second absorption peak according to the distance between dark meta-molecules is also observed, suggesting the potential applications to modulation devices. The proposed multi-band absorbers exhibit a quite complicated dependence on the incident angle of EM wave. The absorption of lowest frequency peak is nearly unchanged while those of the higher frequency peaks are more decreased when the incident angle is increased. Our work is expected to contribute a new way for creating multi-band MPAs, not only in the far-infrared region but also at other frequencies, and to be applied to various potential devices such as multi-frequency filters and single/multi-mode switches.

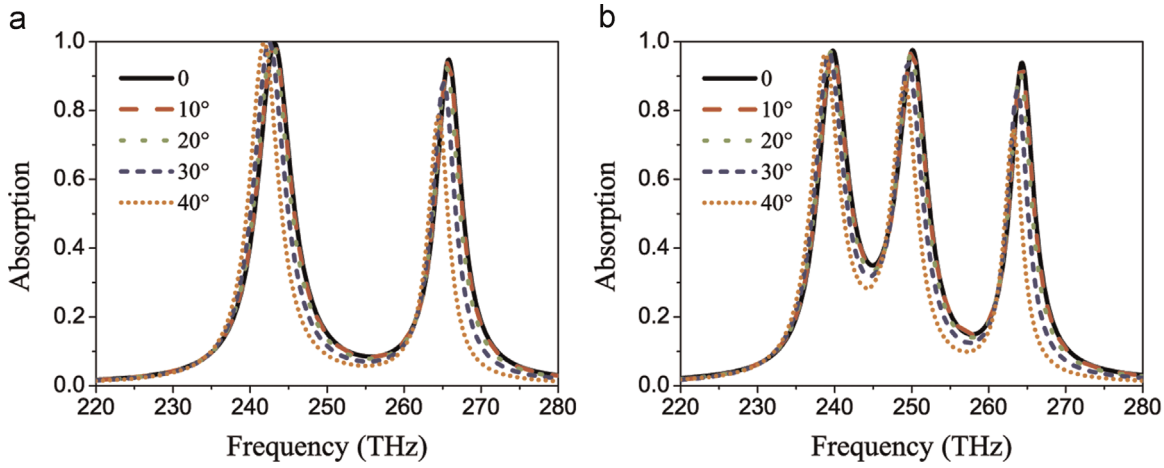

Fig. 6. Dependence of absorption spectra on the incident angle θ of EM wave for (a) the CWTA and (b) CWQA for $s=50$ nm.

Acknowledgment

This work was supported by the ICT R&D Program of MSIP/IITP, Korea (KCA-2013-005-038-001).

References

[1] D.R. Smith, W.J. Padilla, D.C. Vier, S.C. Nemat-Nasser, S. Schultz, Composite medium with simultaneously negative permeability and permittivity, Phys. Rev. Lett. 84 (2000) 4184–4187.
[2] V.D. Lam, J.B. Kim, S.J. Lee, Y.P. Lee, Left-handed behavior of combined and fishnet structures, J. Appl. Phys. 103 (2008) 033107.
[3] L. Gao, K. Shigeta, A. Vazquez-Guardado, C.J. Progler, G.R. Bogart, J.A. Rogers, D. Chanda, Nanoimprinting techniques for large-area three-dimensional negative index metamaterials with operation in the visible and telecom bands, ACS Nano 8 (2014) 5535–5542.
[4] D. Schurig, J.J. Mock, B.J. Justice, S.A. Cummer, J.B. Pendry, A.F. Starr, D.R. Smith, Metamaterial electromagnetic cloak at microwave frequencies, Science 314 (2006) 977–980.
[5] G. Pawlik, K. Tarnowski, W. Walasik, A.C. Mitus, I.C. Khoo, Infrared cylindrical cloak in nanosphere dispersed liquid crystal metamaterial, Opt. Lett. 37 (2012) 1847–1849.
[6] N. Fang, H. Lee, C. Sun, X. Zhang, Subdiffraction-limited optical imaging with a silver superlens, Science 308 (2005) 534–537.
[7] C.P. Scarborough, Z.H. Jiang, D.H. Werner, C. Rivero-Baleine, C. Drake, Experimental demonstration of an isotropic metamaterial super lens with negative unity permeability at 8.5 MHz, Appl. Phys. Lett. 101 (2012) 014101.
[8] N.I. Landy, S. Sajuyigbe, J.J. Mock, D.R. Smith, W.J. Padilla, Perfect metamaterial absorber, Phys. Rev. Lett. 100 (2008) 207402.
[9] K. Aydin, V.E. Ferry, R.M. Briggs, H.A. Atwater, Broadband polarization-independent resonant light absorption using ultrathin plasmonic super absorbers, Nat. Commun. 2 (2011) 517.
[10] C.M. Watts, D. Shrekenhamer, J. Montoya, G. Lipworth, J. Hunt, T. Sleasman, S. Krishna, D.R. Smith, W.J. Padilla, Terahertz compressive imaging with metamaterial spatial light modulators, Nat. Photon. 8 (2014) 605–609.
[11] N. Liu, M. Mesch, T. Weiss, M. Hentschel, H. Giessen, Infrared perfect absorber and its application as plasmonic sensor, Nano Lett. 10 (2010) 2342–2348.
[12] Y.J. Yoo, H.Y. Zheng, Y.J. Kim, J.Y. Rhee, J.-H. Kang, K.W. Kim, H. Cheong, Y. H. Kim, Y.P. Lee, Flexible and elastic metamaterial absorber for low frequency, based on small-size unit cell, Appl. Phys. Lett. 105 (2014) 041902.
[13] P.V. Tuong, J.W. Park, J.Y. Rhee, K.W. Kim, W.H. Jang, H. Cheong, Y.P. Lee, Polarization-insensitive and polarization-controlled dual-band absorption in metamaterials, Appl. Phys. Lett. 102 (2013) 081122.
[14] L. Huang, D.R. Chowdhury, S. Ramani, M.T. Reiten, S.-N. Luo, A.J. Taylor, H.-T. Chen, Experimental demonstration of terahertz metamaterial absorbers with a broad and flat high absorption band, Opt. Lett. 37 (2012) 154–156.
[15] F. Ding, Y. Cui, X. Ge, Y. Jin, S. He, Ultra-broadband microwave metamaterial absorber, Appl. Phys. Lett. 100 (2012) 103506.
[16] J. Zhu, Z. Ma, W. Sun, F. Ding, Q. He, L. Zhou, Y. Ma, Ultra-broadband terahertz metamaterial absorber, Appl. Phys. Lett. 105 (2014) 021102.
[17] S. Liu, H. Chen, T.J. Cui, A broadband terahertz absorber using multi-layer stacked bars, Appl. Phys. Lett. 106 (2015) 151601.
[18] S.E. Harris, Electromagnetically induced transparency, Phys. Today 50 (7) (1997) 36–42.
[19] M. Fleischhauer, A. Imamoglu, J.P. Marangos, Electromagnetically induced transparency: optics in coherent media, Rev. Mod. Phys. 77 (2005) 633–673.
[20] S. Zhang, D.A. Genov, Y. Wang, M. Liu, X. Zhang, Plasmon-induced transparency in metamaterials, Phys. Rev. Lett. 101 (2008) 047401.
[21] V.T.T. Thuy, N.T. Tung, J.W. Park, V.D. Lam, Y.P. Lee, J.Y. Rhee, Highly dispersive transparency in coupled metamaterials, J. Opt. 12 (2010) 115102.
[22] X.R. Jin, Y. Lu, H. Zheng, Y.P. Lee, J.Y. Rhee, K.W. Kim, W.H. Jang, Plasmonic electromagnetically-induced transparency in metamaterial based on second-order plasmonic resonance, Opt. Commun. 284 (2011) 4766–4768.
[23] M.A. Ordal, L.L. Long, R.J. Bell, S.E. Bell, R.R. Bell, R.W. AlexanderJr., C.A. Ward, Optical properties of the metals Al, Co, Cu, Au, Fe, Pb, Ni, Pd, Pt, Ag, Ti, and W in the infrared and far infrared, Appl. Opt. 22 (1983) 1099–1119.
[24] G. Ghosh, Dispersion-equation coefficients for the refractive index and birefringence of calcite and quartz crystals, Opt. Commun. 163 (1–3) (1999) 95–102.
[25] ⟨www.cst.com⟩.
[26] X. Liu, T. Starr, A.F. Starr, W.J. Padilla, Infrared spatial and frequency selective metamaterial with near-unity absorbance, Phys. Rev. Lett. 104 (2010) 207403.
[27] J. Hao, J. Wang, X. Liu, W.J. Padilla, L. Zhou, M. Qiu, High performance optical absorber based on a plasmonic metamaterial, Appl. Phys. Lett. 96 (2010) 251104.
[28] P.K. Jha, M. Mrejen, J. Kim, C. Wu, X. Yin, Y. Wang, X. Zhang, Interacting dark resonances with plasmonic meta-molecules, Appl. Phys. Lett. 105 (2014) 111109.
[29] N. Liu, M. Hentschel, T. Weiss, A.P. Alivisatos, H. Giessen, Three-dimensional plasmon rulers, Science 332 (2011) 1407–1410.
[30] M. Miyata, J. Hirohata, Y. Nagasaki, J. Takahara, Multi-spectral plasmon induced transparency via in-plane dipole and dual-quadrupole coupling, Opt. Express 22 (2014) 11399–11406.
[31] J. Zhou, E.N. Economon, T. Koschny, C.M. Soukoulis, Unifying approach to left-handed material design, Opt. Lett. 31 (2006) 3620–3622.
[32] N.T. Tung, D.T. Viet, B.S. Tung, N.V. Hieu, P. Lievens, V.D. Lam, Broadband negative permeability by hybridized cut-wire pair metamaterials, Appl. Phys. Express 5 (2012) 112001.